NANO LETTERS

pubs.acs.org/NanoLett

Letter

Size Dependent Specific Heat Capacity of PbSe Nanocrystals

Kai Gu, Heng Wu, Jiaming Su, Peihan Sun, Ping-Heng Tan, and Haizheng Zhong*

Cite This: *Nano Lett.* 2024, 24, 4038−4043

Read Online

ACCESS | Metrics & More | Article Recommendations | Supporting Information

ABSTRACT: Specific heat capacity is one of the most fundamental thermodynamic properties of materials. In this work, we measured the specific heat capacity of PbSe nanocrystals with diameters ranging from 5 to 23 nm, and its value increases significantly from 0.2 to 0.6 J g^{-1} $°C^{-1}$. We propose a mass assignment model to describe the specific heat capacity of nanocrystals, which divides it into four parts: electron, inner, surface, and ligand. By eliminating the contribution of ligand and electron specific heat capacity, the specific heat capacity of the inorganic core is linearly proportional to its surface-to-volume ratio, showing the size dependence. Based on this linear relationship, surface specific heat capacity accounts for 40−60% of the specific heat capacity of nanocrystals with size decreasing. It can be attributed to the uncoordinated surface atoms, which is evidenced by the appearance of extra surface phonons in Raman spectra and ab initio molecular dynamics (AIMD) simulations.

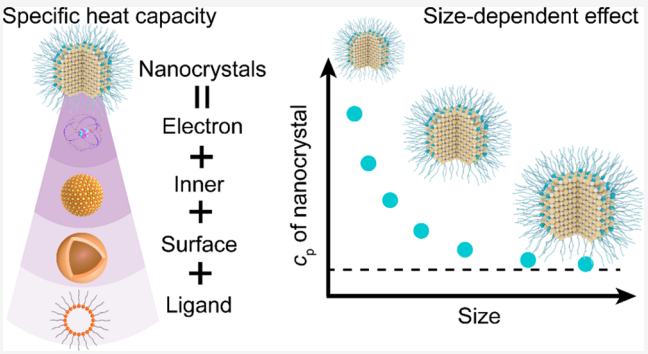

KEYWORDS: *specific heat capacity, semiconductor nanocrystal, size dependence, surface phonon*

In comparison with bulk materials, nanocrystals show a wide range of size dependent effects including optical,[1−3] magnetic,[4,5] catalytic,[6,7] and thermodynamic properties.[8−11] With the development of nanocrystal based photonic and optoelectronic devices, stability becomes an urgent issue to initialize industrialization.[12,13] Temperature increase is a commonly observed phenomenon related to the thermal stability of nanocrystal devices.[14−16] Specific heat capacity, termed as heat capacity per unit of mass, is one of the most fundamental thermodynamic properties of materials.[17,18] In principle, temperature increase is inversely proportional to heat capacity under certain conditions, which is a key parameter to design highly stable electronic devices. Early works and simulations have shown that the specific heat capacity of metal nanocrystals increases by 10% to 40% at low and room temperatures.[19−23] The enhanced specific heat capacity of metal nanocrystals can be attributed to the increase of surface-to-volume ratio, which can explain the decrease of Debye temperature induced by extra surface phonons.[24−28] In comparison, the specific heat capacity of semiconductor nanocrystals has received limited attention. Here, we report the size dependence in the specific heat capacity of colloidal PbSe nanocrystals.

Colloidal nanocrystals consist of an inorganic core and an organic ligand, where the specific heat capacity of the ligand is usually larger than that of the inorganic core. From a microscopic perspective, a phonon describes the vibration of solids, which is correlated with its specific heat capacity.[29] Because of the high surface-to-volume ratio of nanocrystals, surface phonons induced by uncoordinated surface atoms play a vital role in determining their thermodynamic properties.[30] As shown in Figure 1, the specific heat capacity of colloidal nanocrystals is different from that of bulk materials and is determined by four parts: electron, inner, surface, and ligand. The proportion of specific heat capacity of each part is assigned by mass. The specific heat capacity of nanocrystals is expected to exhibit size dependence, because the content of ligands and the ratio of surface atoms are size related.

A series of monodisperse PbSe nanocrystals with different sizes were synthesized via the previously reported hot injection method. Transmission electron microscope (TEM) images and the corresponding size distributions are shown in Figure 2a−c and Figure S1 and S2. Synthesis parameters are listed in Table S1. Figure 2d shows the specific heat capacity of PbSe nanocrystals for different sizes (refer to the Methods for test details and calculations). The specific heat capacity of PbSe nanocrystals decreases with increasing size. For example, the specific heat capacity of PbSe nanocrystals with a diameter of 5 nm at 25 °C is 0.61 J g^{-1} $°C^{-1}$, which is three times bigger than that of PbSe nanocrystals with a diameter of 23 nm (0.19 J g^{-1} $°C^{-1}$). In addition, the specific heat capacity of PbSe

Received: February 28, 2024
Revised: March 19, 2024
Accepted: March 19, 2024
Published: March 21, 2024

ACS Publications

© 2024 American Chemical Society

https://doi.org/10.1021/acs.nanolett.4c01021
Nano Lett. 2024, 24, 4038−4043

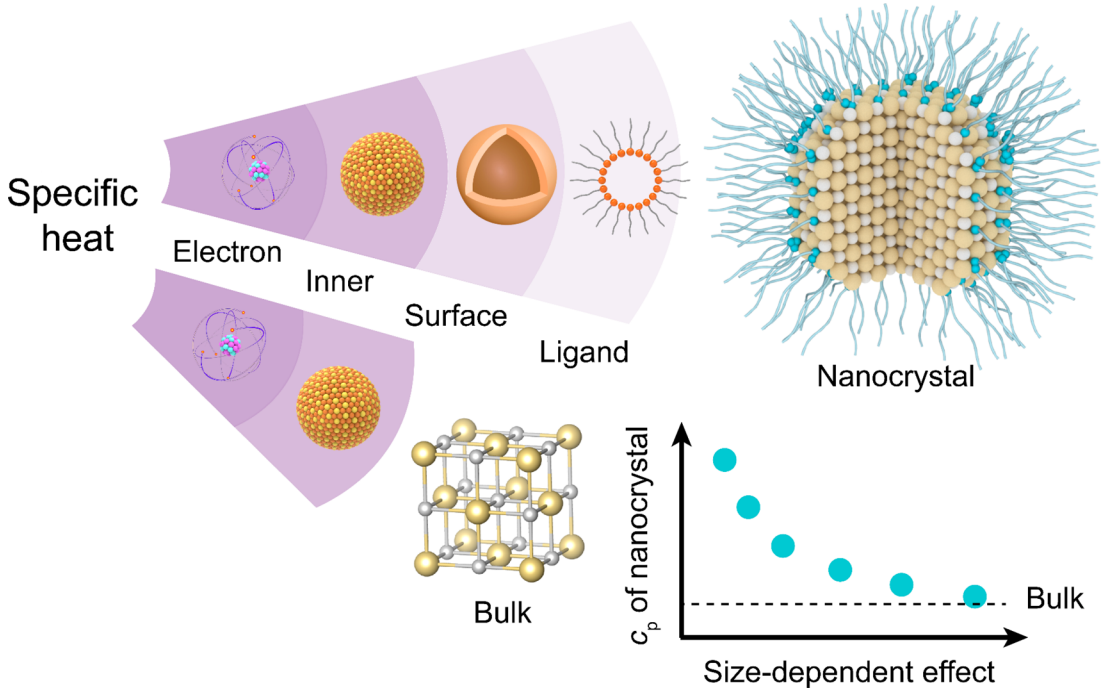

Figure 1. Schematic illustration of the components of specific heat capacity for nanocrystals and bulk materials and the size-dependent effect of nanocrystals.

nanocrystals is almost linearly dependent on the temperature, and its slope decreases with increasing size (Figure S3 and Table S2). According to our proposed mass assignment model, the specific heat capacity of nanocrystals can be described in equations 1 and 2

$$c_p(T, D) = \alpha c_l(T) + (1 - \alpha)c_{nano}(T, D) + c_e(T) \quad (1)$$

$$c_{nano}(T, D) = \beta(D)c_s(T) + [1 - \beta(D)]c_i(T) \quad (2)$$

where c_p is the specific heat capacity of nanocrystals, α is the weight fraction of the ligand, c_l is the specific heat capacity of the ligand, and c_{nano} is the specific heat capacity of bare nanocrystals without ligand coverage. c_e is the electron heat capacity and $c_e = \gamma T$, where $\gamma = 3.829 \times 10^{-5}$ J·g^{-1}·K^{-2} (derived from Figure 2e). β is the fraction of surface atoms to the total number of atoms, D is the diameter of nanocrystals, and c_s is the specific heat capacity of surface atoms. c_i is the specific heat capacity of the inner core and $c_i = c_b$, where c_b is the specific heat capacity of the bulk.

As shown in equation 1, the specific heat capacity of nanocrystals can be split into four parts based on the mass fraction of each component. Based on the measurement of the Quantum Design-Physical Property Measurement System (PPMS) at 2−20 K, the specific heat capacity coefficient of electrons (γ) was obtained from the intercept by fitting the $c_p/T - T^2$ line,[24] as shown in Figure 2e. c_e is about one-sixtieth smaller than c_p at 100 °C for small size nanocrystals. Besides, the mass fraction and specific heat capacity of the ligand can be determined by thermogravimetric analysis (TGA). Based on the TGA curve of PbSe powder in Figure S4a, no thermal decomposition was observed before 600 °C. Therefore, we calculated the mass fraction of ligands (α) from the TGA curve of PbSe nanocrystals (Figure S4b). Figure 2f shows the calculated mass fraction of the ligand for different sizes of PbSe nanocrystals. In addition, we can also clarify the type of ligand from the first-order derivative of TGA (DTG) curves and X-ray photoelectron spectroscopy (XPS). Figure S5a and S5b shows TGA and DTG plots of typical nanocrystals and possible ligands, respectively. Table S3 summarizes the decomposition temperatures (Figure S5c) and characteristic decomposition peaks. The decomposition mode of lead oleate is very similar to that of the PbSe nanocrystals. As shown in Figure S5d, the existence of oleate anion was also confirmed by Fourier transform infrared spectroscopy (FTIR). According to the XPS measurements (Figure S6), the resulting PbSe nanocrystals contain very slight N and P elements, which suggests the absence of oleylamine and trioctylphosphine on the surface. Therefore, the specific heat capacity of lead oleate was measured as c_l, as shown in Figure S7. The specific heat capacity of lead oleate is more than six times larger than that of PbSe bulk and shows a large increase with temperature. After determining the c_e, c_l, and α, the c_{nano} at different temperatures can be calculated from equation 1 (refer to the Methods for details). c_{nano} is slightly varied with temperature (Figure S8), suggesting that the large variation of c_p with temperature is attributable to the ligand. By rewriting equation 2, equation 3 clearly shows the linear proportion between c_{nano} and β at a given temperature.

$$c_{nano}(T, D) = [c_s(T) - c_b(T)]\beta(D) + c_b(T) \quad (3)$$

β is related to the morphology of the nanocrystals and the number of atomic layers on the surface. $\beta(D)$ functions were calculated for spherical and cubic nanocrystals considering different thicknesses of the surface (Figure S9). To minimize the error resulting from the morphology variation, the $\beta(D)$ function is used to consider a single layer of surface atoms (n = 1), as shown in Figure 2g. Figure 2h shows the size dependence of c_{nano}. c_{nano} is linear with β when the diameter of the nanocrystals is less than 20 nm. The c_{nano} of cubic PbSe nanocrystals is faster approaching c_b when the diameter of nanocrystals is larger than 20 nm, due to the self-assembly of homogeneous nanocrystals (Figure S10). The size-dependent

https://doi.org/10.1021/acs.nanolett.4c01021
Nano Lett. 2024, 24, 4038−4043

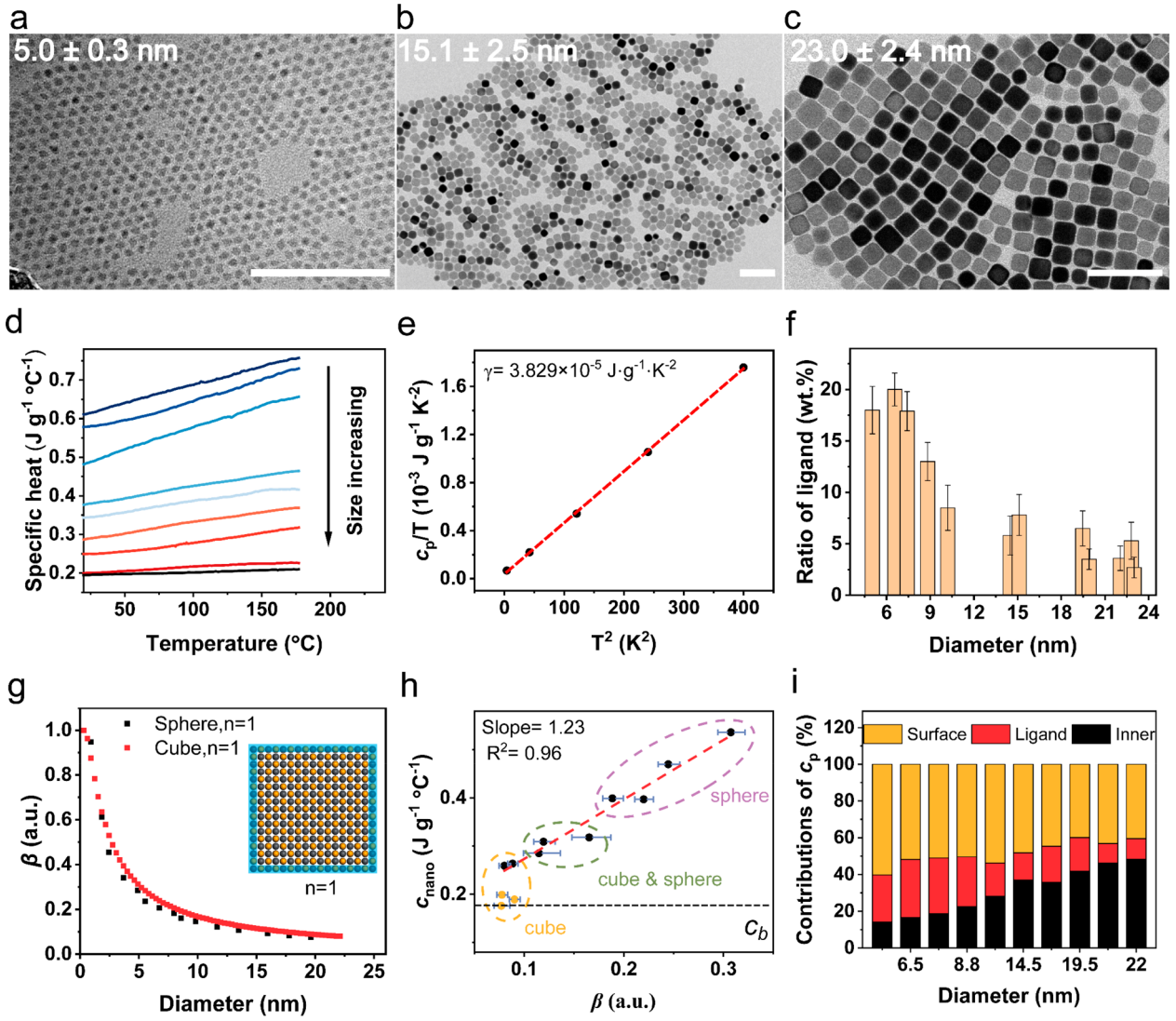

Figure 2. Characterization and specific heat capacity calculation of PbSe nanocrystals. (a−c) TEM images of the as-synthesized PbSe nanocrystals. The scale bar is 100 nm. (d) Plot of the specific heat capacity versus temperature for PbSe nanocrystals with different sizes. (e) Plot of the low-temperature specific heat capacity of PbSe nanocrystals. γ is obtained from the intercept of the fitted curve. (f) Mass fraction of ligands (α) for different sizes of PbSe nanocrystals. The error bars are the standard deviation of three measurements. (g) The $\beta(D)$ function for spherical and cubic PbSe nanocrystals with one surface atom layer (n = 1). Inset: schematic of a cubic nanocrystal with one surface atom layer. (h) Size dependence of c_{nano} for PbSe nanocrystals. The colors of the dashed circles represent the different morphologies of PbSe nanocrystals. The error bars are derived from the size distribution. (i) Contributions of the specific heat capacity of ligands, surface, and inner of core for different PbSe nanocrystal samples.

effect of c_{nano} of PbS nanocrystals was also measured to verify the versatility of the model (Figure S11). c_s can be derived from the slopes of the fitted curve in Figure 2h. Figure 2i shows the percentage of the specific heat capacity of each part for PbSe nanocrystals (refer to the Methods for details). The specific heat capacities of the ligand and surface are dominant in small nanocrystals, leading to the enhancement of the specific heat capacity of nanocrystals.

To further investigate the enhancement of surface specific heat capacity, Raman spectra of PbSe nanocrystals with different sizes were performed, as shown in Figure 3a. The peaks for each sample were subject to Lorentzian fitting (Figure S12), and the positions and corresponding vibrational modes of all fitted peaks were summarized in Table S4. The asymmetric shoulder near the longitudinal optical (LO) mode is attributed to the surface phonon (SP) mode.[31] Compared with bulk materials, nanocrystals show additional SP modes due to insufficient coordination of surface atoms, which can enhance the specific heat capacity of the nanocrystals. In addition the LO peak shifts to higher wavenumbers as the nanocrystal size decreases (inset of Figure 3a). A shift of the LO mode to lower wavenumbers was also observed under high-power excitation, which may be related to the photothermal effect of PbSe nanocrystals (Figure S13). Furthermore, the vibrational properties of PbSe nanocrystals were investigated by using AIMD simulations. As shown in Figure 3b, the phonon density of states of PbSe nanocrystals consisting of 216 atoms (Figure S14a) was calculated at 300 K, with 10 ps, where the nanocrystals were divided into three layers (inset of Figure 3b). The positions of the transverse optical (TO) mode and the LO are consistent with the results of Raman spectra. Compared to the density of states of the core atoms, the surface atoms exhibit a broadened density of states.[30] Figure 3c visualizes the evolution of the density of states, where $\Delta g(\omega)$ =

https://doi.org/10.1021/acs.nanolett.4c01021
Nano Lett. 2024, 24, 4038−4043

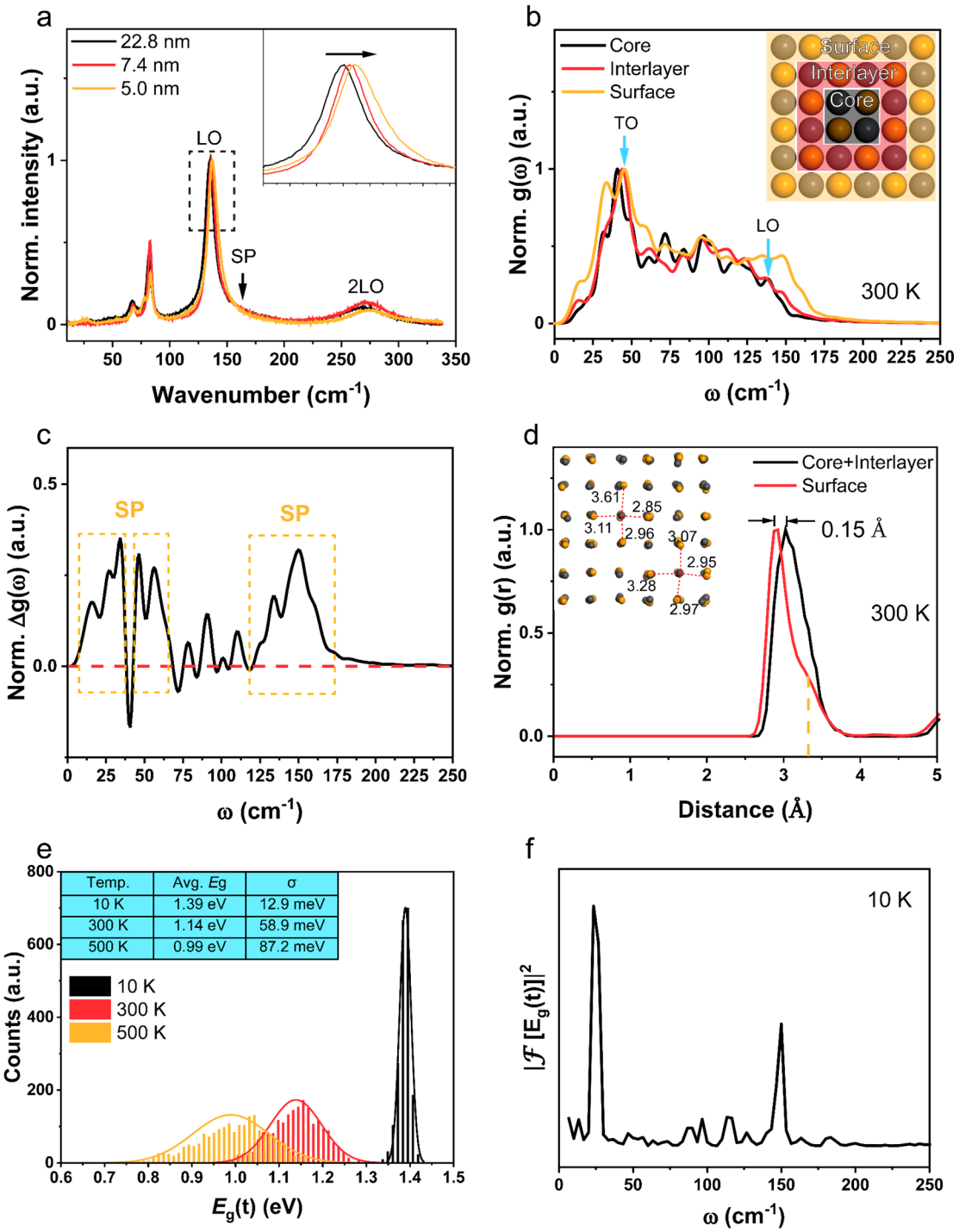

Figure 3. Vibration analysis of PbSe nanocrystals. (a) Normalized Raman spectra of PbSe nanocrystals. The inset is an enlarged diagram of the LO mode. (b) Phonon density of states of PbSe nanocrystals with different atomic layers calculated at 300 K (10 ps trajectory). The inset shows PbSe nanocrystals consisting of 216 atoms. (c) Differences between the phonon density of states for the surface and the core. (d) Radial distribution functions of different atomic layers in PbSe nanocrystals. The inset shows the characteristic bond lengths (Å) of the surface atoms at a certain frame. (e) Time-dependent band gap distribution of PbSe nanocrystals at different temperatures. The inset table is a record of the average band gap and the standard deviation at different temperatures. (f) Power spectrum of $E_g(t)$ at 10 K.

$g_{surface}(\omega) - g_{core}(\omega)$. Additional SP modes are observed near the LO mode (135 cm^{-1}) and the TO mode (47 cm^{-1}). Pb- and Se-rich (111) surfaces exhibit more softening by projecting the surface phonon density of states of different facets (Figure S15). Extra SP modes of PbS nanocrystals were also observed in Figure S16. The positions of the SP mode near the LO mode are consistent with those in Raman spectra, while the TO mode has a low resolution in Raman spectra (Table S4). The Pb atoms are mainly vibrating at low frequencies, and Se atoms are vibrating at high frequencies in the nanocrystals, due to the greater mass of the Pb atoms than the Se atoms (Figure S17).[32] The amplitude of Pb atoms is greater than that of Se atoms, and the amplitude of surface atoms is greater than that of core atoms (Figure S18a). The slight shift of the TO and

https://doi.org/10.1021/acs.nanolett.4c01021
Nano Lett. 2024, 24, 4038−4043

LO peaks toward lower wavenumbers and the overall density of states increase at high temperatures (Figure S18b), which agrees with the slight increase in c_{nano} at high temperatures. The density of states increases for small-sized nanocrystals (Figure S18c). Additional SP modes in PbSe nanocrystals may be related with asymmetric vibrations of surface atoms.[30] Figure 3d shows the radial distribution function of the surface and internal atoms, where the bond lengths of the surface atoms are 0.15 Å smaller than those of the internal atoms. Surface atoms have two types of bond lengths: one part is less than 3 Å, and the other part is greater than 3 Å (the inset shows the bond lengths of the atoms at a certain frame). This asymmetric surface vibration is weakened at high temperatures (Figure S19). The electron−phonon coupling property is important for optoelectronic materials. The band gaps for each frame were calculated from the AIMD traces of the PbSe nanocrystals. Figure 3e shows the distribution of the band gap versus time $E_g(t)$ at different temperatures. The band gap of the nanocrystals becomes smaller, and the distribution is broadened at high temperatures. Dramatic fluctuations of the band gap indicate the dependence of the electronic structure on the atomic positions of the nanocrystals, suggesting strong electron−phonon coupling.[32] The power spectrum density $|\mathcal{F}[E_g(t)]|^2$ of the time-dependent bandgap was calculated, where $\mathcal{F}$ denotes the Fourier transform, as shown in Figure 3f. The peaks in the power spectrum density indicate that phonons at these frequencies are actively driving the energy state fluctuations. Figure 3f shows that electrons couple to phonons with wavenumbers of 23−26 cm^{-1} and 150 cm^{-1}, exactly corresponding to the SP mode of PbSe nanocrystals.

Softened and extra surface phonons lead to a larger specific heat capacity of the nanocrystals than its bulk. Size dependence of the specific heat capacity of nanocrystals implies that the specific heat capacity can be controlled by varying their size. Larger values of the specific heat capacity are useful to resist the influence of heat in optoelectronic devices. Therefore, the specific heat capacity of nanocrystals is undoubtedly an important parameter to design high-performance and high-stability (optoelectronic) devices. However, photothermal applications may require a balanced specific heat capacity to achieve a high temperature increase.

In conclusion, we synthesized a series of homogeneous monodisperse PbSe nanocrystals and investigated the size dependence of their specific heat capacity. By considering the effects of ligands, electrons, surface, and inner, we have developed a model to describe the enhancement and size dependence of the specific heat capacity of nanocrystals. The results show that each part contributes differently to the specific heat capacity of nanocrystals with size decreasing (ligand, from 10% to 25%; surface, from 40% to 60%; inner, from 50% to 15%), while the contribution of electron specific heat capacity is only 1%. Most importantly, c_{nano} is inversely proportional to the size-related β (surface-to-volume ratio). This model is also applicable to describe the size dependence of the specific heat capacity in PbS nanocrystals. Furthermore, by using Raman spectroscopy and AIMD simulations, it was revealed that extra SP modes near the TO and LO modes of nanocrystals may be related to the asymmetric vibrations of the surface atoms, which mainly accounts for the enhancement of the specific heat capacity of the nanocrystals.

■ ASSOCIATED CONTENT

Supporting Information

The Supporting Information is available free of charge at https://pubs.acs.org/doi/10.1021/acs.nanolett.4c01021.

Synthesis and characterizations of samples; calculation details of the mass assignment model; AIMD simulation details; TEM images and size distributions of the samples; TGA, FTIR, XPS, XRD, and specific heat capacity curves of samples; Raman spectra of PbSe nanocrystals; phonon density of states, radial distribution functions, and root-mean-square fluctuations of nanocrystals (PDF)

■ AUTHOR INFORMATION

Corresponding Author

Haizheng Zhong − *MIIT Key Laboratory for Low-Dimensional Quantum Structure and Devices, School of Materials Science & Engineering, Beijing Institute of Technology, Beijing 100081, P. R. China;* orcid.org/0000-0002-2662-7472; Email: hzzhong@bit.edu.cn

Authors

Kai Gu − *MIIT Key Laboratory for Low-Dimensional Quantum Structure and Devices, School of Materials Science & Engineering, Beijing Institute of Technology, Beijing 100081, P. R. China*

Heng Wu − *State Key Laboratory of Superlattices and Microstructures, Institute of Semiconductors, Chinese Academy of Sciences, Beijing 100083, P. R. China*

Jiaming Su − *MIIT Key Laboratory for Low-Dimensional Quantum Structure and Devices, School of Materials Science & Engineering, Beijing Institute of Technology, Beijing 100081, P. R. China*

Peihan Sun − *MIIT Key Laboratory for Low-Dimensional Quantum Structure and Devices, School of Materials Science & Engineering, Beijing Institute of Technology, Beijing 100081, P. R. China*

Ping-Heng Tan − *State Key Laboratory of Superlattices and Microstructures, Institute of Semiconductors, Chinese Academy of Sciences, Beijing 100083, P. R. China;* orcid.org/0000-0001-6575-1516

Complete contact information is available at: https://pubs.acs.org/10.1021/acs.nanolett.4c01021

Author Contributions

H.Z. conceived the project. K.G., J.S., and P.S. synthesized the PbSe and PbS nanocrystals. K.G. conceived and developed the model and performed the AIMD simulations. H.W. and P.-H.T. measured Raman spectra of nanocrystals. K.G. and H.Z. analyzed the data and wrote the manuscript with input of other authors.

Notes

The authors declare no competing financial interest.

■ ACKNOWLEDGMENTS

This work was supported by Natural Science Foundation of China (U23A20683, H.Z.). We thank Experimental Center of Advanced Materials of Beijing Institute of Technology. The authors thank Prof. Yulong Liu for his help on the interpretation of Raman spectra.

REFERENCES

(1) Alivisatos, A. P. Semiconductor Clusters, Nanocrystals, and Quantum Dots. *Science* **1996**, *271* (5251), 933−937.
(2) Moreels, I.; Lambert, K.; Smeets, D.; De Muynck, D.; Nollet, T.; Martins, J. C.; Vanhaecke, F.; Vantomme, A.; Delerue, C.; Allan, G.; et al. Size-Dependent Optical Properties of Colloidal PbS Quantum Dots. *ACS Nano* **2009**, *3* (10), 3023−3030.
(3) Yuan, M.; Liu, M.; Sargent, E. H. Colloidal quantum dot solids for solution-processed solar cells. *Nature Energy* **2016**, *1* (3), No. 16016.
(4) Chen, J. P.; Sorensen, C. M.; Klabunde, K. J.; Hadjipanayis, G. C.; Devlin, E.; Kostikas, A. Size-dependent magnetic properties of $MnFe_2O_4$ fine particles synthesized by coprecipitation. *Physical Review B* **1996**, *54* (13), 9288−9296.
(5) Park, T.-J.; Papaefthymiou, G. C.; Viescas, A. J.; Moodenbaugh, A. R.; Wong, S. S. Size-Dependent Magnetic Properties of Single-Crystalline Multiferroic $BiFeO_3$ Nanoparticles. *Nano Letters* **2007**, *7* (3), 766−772.
(6) Rao, C. N. R.; Kulkarni, G. U.; Thomas, P. J.; Edwards, P. P. Size-Dependent Chemistry: Properties of Nanocrystals. *Chemistry − A European Journal* **2002**, *8* (1), 28−35.
(7) Muravev, V.; Parastaev, A.; van den Bosch, Y.; Ligt, B.; Claes, N.; Bals, S.; Kosinov, N.; Hensen, E. J. M. Size of cerium dioxide support nanocrystals dictates reactivity of highly dispersed palladium catalysts. *Science* **2023**, *380* (6650), 1174−1179.
(8) Goldstein, A. N.; Echer, C. M.; Alivisatos, A. P. Melting in Semiconductor Nanocrystals. *Science* **1992**, *256* (5062), 1425−1427.
(9) Neeleshwar, S.; Chen, C. L.; Tsai, C. B.; Chen, Y. Y.; Chen, C. C.; Shyu, S. G.; Seehra, M. S. Size-dependent properties of CdSe quantum dots. *Physical Review B* **2005**, *71* (20), No. 201307.
(10) Anufriev, R.; Gluchko, S.; Volz, S.; Nomura, M. Quasi-Ballistic Heat Conduction due to Lévy Phonon Flights in Silicon Nanowires. *ACS Nano* **2018**, *12* (12), 11928−11935.
(11) Shi, C.; Beecher, A. N.; Li, Y.; Owen, J. S.; Leu, B. M.; Said, A. H.; Hu, M. Y.; Billinge, S. J. L. Size-Dependent Lattice Dynamics of Atomically Precise Cadmium Selenide Quantum Dots. *Phys. Rev. Lett.* **2019**, *122* (2), No. 026101.
(12) Woo, S.-J.; Kim, J. S.; Lee, T.-W. Characterization of stability and challenges to improve lifetime in perovskite LEDs. *Nature Photonics* **2021**, *15* (9), 630−634.
(13) García de Arquer, F. P.; Talapin, D. V.; Klimov, V. I.; Arakawa, Y.; Bayer, M.; Sargent, E. H. Semiconductor quantum dots: Technological progress and future challenges. *Science* **2021**, *373* (6555), No. eaaz8541.
(14) Jeong, B. G.; Park, Y.-S.; Chang, J. H.; Cho, I.; Kim, J. K.; Kim, H.; Char, K.; Cho, J.; Klimov, V. I.; Park, P.; et al. Colloidal Spherical Quantum Wells with Near-Unity Photoluminescence Quantum Yield and Suppressed Blinking. *ACS Nano* **2016**, *10* (10), 9297−9305.
(15) Tang, J.; Li, F.; Yang, G.; Ge, Y.; Li, Z.; Xia, Z.; Shen, H.; Zhong, H. Reducing the Chromaticity Shifts of Light-Emitting Diodes Using Gradient-Alloyed $Cd_xZn_{1-x}Se_yS_{1-y}$@ZnS Core Shell Quantum Dots with Enhanced High-Temperature Photoluminescence. *Advanced Optical Materials* **2019**, *7* (10), No. 1801687.
(16) Moon, H.; Lee, C.; Lee, W.; Kim, J.; Chae, H. Stability of Quantum Dots, Quantum Dot Films, and Quantum Dot Light-Emitting Diodes for Display Applications. *Adv. Mater.* **2019**, *31* (34), No. 1804294.
(17) Ginnings, D. C.; Furukawa, G. T. Heat Capacity Standards for the Range 14 to 1200° K. *J. Am. Chem. Soc.* **1953**, *75* (3), 522−527.
(18) Piespergen, U. Chapter 3 Heat Capacity and Debye Temperatures. In *Semiconductors and Semimetals*; Willardson, R. K., Beer, A. C. Eds.; Elsevier: 1966; Vol. *2*, pp 49−60.
(19) Sun, N. X.; Lu, K. Heat-capacity comparison among the nanocrystalline, amorphous, and coarse-grained polycrystalline states in element selenium. *Physical Review B* **1996**, *54* (9), 6058−6061.
(20) Rupp, J.; Birringer, R. Enhanced specific-heat-capacity (c_p) measurements (150–300 K) of nanometer-sized crystalline materials. *Physical Review B* **1987**, *36* (15), 7888−7890.
(21) Wolf, D.; Wang, J.; Phillpot, S. R.; Gleiter, H. Phonon-Induced Anomalous Specific Heat of a Nanocrystalline Model Material by Computer Simulation. *Phys. Rev. Lett.* **1995**, *74* (23), 4686−4689.
(22) Piekarz, P.; Łażewski, J.; Jochym, P. T.; Sternik, M.; Parlinski, K. Vibrational properties and stability of FePt nanoalloys. *Physical Review B* **2017**, *95* (13), No. 134303.
(23) Meyer, R.; Lewis, L. J.; Prakash, S.; Entel, P. Vibrational properties of nanoscale materials: From nanoparticles to nanocrystalline materials. *Physical Review B* **2003**, *68* (10), No. 104303.
(24) Lei, H.; Li, J.; Luo, J. Surface specific heats of metal nanocrystals at low temperatures. *Nanoscale* **2015**, *7* (15), 6762−6766.
(25) Luo, W.; Hu, W.; Xiao, S. Size Effect on the Thermodynamic Properties of Silver Nanoparticles. *The Journal of Physical Chemistry C* **2008**, *112* (7), 2359−2369.
(26) Huang, M.-J.; Chang, T.-M.; Liu, C.-K.; Yu, C.-K. A theoretical study of the specific heat and Debye temperature of low-dimensional materials. *Int. J. Heat Mass Transfer* **2008**, *51* (17), 4470−4479.
(27) Ong, W.-L.; Rupich, S. M.; Talapin, D. V.; McGaughey, A. J. H.; Malen, J. A. Surface chemistry mediates thermal transport in three-dimensional nanocrystal arrays. *Nat. Mater.* **2013**, *12* (5), 410−415.
(28) Jansen, M.; Tisdale, W. A.; Wood, V. Nanocrystal phononics. *Nat. Mater.* **2023**, *22* (2), 161−169.
(29) Harker, A. H. The physics of phonons, 2nd edition. *Contemporary Physics* **2022**, *63* (4), 337−337.
(30) Bozyigit, D.; Yazdani, N.; Yarema, M.; Yarema, O.; Lin, W. M. M.; Volk, S.; Vuttivorakulchai, K.; Luisier, M.; Juranyi, F.; Wood, V. Soft surfaces of nanomaterials enable strong phonon interactions. *Nature* **2016**, *531* (7596), 618−622.
(31) Manciu, F. S.; Sahoo, Y.; Carreto, F.; Prasad, P. N. Size-dependent Raman and infrared studies of PbSe nanoparticles. *J. Raman Spectrosc.* **2008**, *39* (9), 1135−1140.
(32) Yazdani, N.; Bozyigit, D.; Vuttivorakulchai, K.; Luisier, M.; Infante, I.; Wood, V. Tuning Electron−Phonon Interactions in Nanocrystals through Surface Termination. *Nano Letters* **2018**, *18* (4), 2233−2242.

https://doi.org/10.1021/acs.nanolett.4c01021
Nano Lett. 2024, 24, 4038−4043